Available online at www.sciencedirect.com
SCIENCE DIRECT
Journal of Catalysis 229 (2005) 97–104
JOURNAL OF CATALYSIS
www.elsevier.com/locate/jcat

Liquid-phase chemoselective hydrogenation of 2-ethylanthraquinone over chromium-modified nanosized amorphous Ni–B catalysts

Jing Fang [a], Xueying Chen [a], Bo Liu [a], Shirun Yan [a], Minghua Qiao [a,*], Hexing Li [b], Heyong He [a], Kangnian Fan [a,*]

[a] *Department of Chemistry and Shanghai Key Laboratory of Molecular Catalysis and Innovative materials, Fudan University, Shanghai 200433, People Republic of China*

[b] *Department of Chemistry, Shanghai Normal University, Shanghai 200234, People's Republic of China*

Received 16 August 2004; revised 15 October 2004; accepted 15 October 2004

Available online 24 November 2004

Abstract

Liquid-phase hydrogenation of 2-ethylanthraquinone to 2-ethylanthrahydroquinone has been investigated over Raney Ni, nanosized amorphous Ni–B, and chromium-modified Ni–B catalysts. It has been found that the amorphous Ni–B and chromium-modified Ni–B catalysts exhibited superior selectivity, whereas the chromium-modified Ni–B catalysts had better activity and selectivity than unmodified Ni–B catalyst. Based on the characterizations, the higher selectivity of the amorphous catalysts is ascribed to the dominant population of the strongly bound hydrogen, which is not reactive for the hydrogenation of the aromatic ring, along with the repulsive interaction between the aromatic ring and the electron-rich Ni due to electron donation from alloying B. The addition of chromium decreased the particle size of the amorphous catalysts, which is beneficial for the improvement of activity. Moreover, surface chromium oxide can function as a Lewis acid, which lowers the π^*_{CO} orbital of the reactant, favoring a carbonyl group-bonded configuration. The best selectivity was achieved over the Ni–Cr–B2 catalyst, where the hydrogenation of the aromatic ring was thoroughly blocked before the saturation of the carbonyl groups.

Keywords: Ni–Cr–B amorphous alloy; 2-Ethylanthraquinone; Hydrogenation; Hydrogen peroxide

1. Introduction

The anthraquinone hydrogenation/oxidation process is by far the most popular route for industrial scale production of H_2O_2, an environmentally friendly oxidant [1–3]. In this famous process, 2-ethylanthrahydroquinone ($eAQH_2$) and 2-ethyltetrahydroanthrahydroquinone (H_4eAQH_2), the "active quinones," produced by reduction of 2-ethylanthraquinone (eAQ) in the presence of a hydrogenation catalyst, are oxidized with oxygen or air to yield H_2O_2, and eAQ and 2-ethyltetrahydroanthraquinone (H_4eAQ) are recovered and used in another cycle (Scheme 1). However, during the hydrogenation step, eAQ may degrade to 2-ethylanthracene (eAT) and 2-ethylanthrone (eAN), and H_4eAQH_2 may be deep hydrogenated to 2-ethyloctahydroanthrahydroquinone (H_8eAQH_2) [4,5]. Such by-products cannot produce H_2O_2, leading to the loss of expensive anthraquinones and fed hydrogen. On the other hand, the oxidation rate of H_4eAQH_2 is much slower than that of $eAQH_2$, resulting in a lower efficiency in H_2O_2 production [6]. Thus a catalyst exhibiting exclusive selectivity in hydrogenating the carbonyl group relative to the aromatic ring is highly desired.

For eAQ hydrogenation, although palladium catalysts show higher selectivity than Raney Ni catalyst, the degradation products are still detected [5]. Furthermore, the palladium-based catalysts are expensive. In a previous work, we reported a rapidly quenched skeletal Ni catalyst showing

* Corresponding authors: Minghua Qiao and Kangnian Fan. Fax: +86 21 65642978.

E-mail addresses: mhqiao@fudan.edu.cn (M. Qiao), knfan@fudan.edu.cn (K. Fan).

0021-9517/$ – see front matter
doi:10.1016/j.jcat.2004.10.014

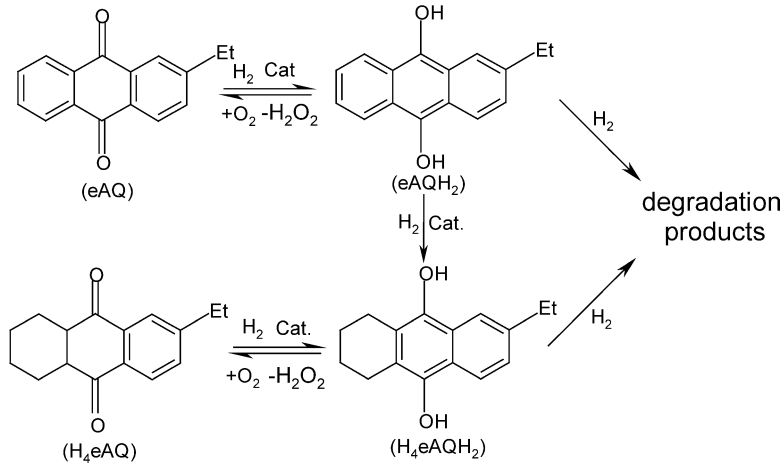

Scheme 1. The hydrogenation and oxidation cycles of eAQ and H_4eAQ.

selectivity superior to that of Raney Ni in eAQ hydrogenation, over which the yield of H_2O_2 reached 97%, about 30% higher than that over Raney Ni. But a detailed chromatographic analysis demonstrated that about 18% of eAQ was converted to H_4eAQ [7].

Recently, amorphous metal alloys have gained much attention as promising novel catalytic materials. Their unique isotropic structure and high concentration of coordinatively unsaturated sites led to catalytic activity and selectivity superior to those of their crystalline counterparts [8–12]. In particular, amorphous alloys prepared by chemical reduction with borohydride (BH_4^-) or hypophosphite ($H_2PO_2^-$) have nanosized morphology and consequently higher surface area and activity than those prepared by the quenching method. On the other hand, chromium has been acknowledged to be an excellent promoter in the selective hydrogenation of the carbonyl group [13–17]. Thus we chose the chromium-modified amorphous Ni–B alloys as the catalysts for eAQ hydrogenation. A brief report on the excellent selectivity of the chromium-modified amorphous Ni–B catalyst has been published elsewhere [18]; here we present a detailed characterization to reveal the modification effect of chromium on the physicochemical properties of the amorphous Ni–B catalyst, based on which the positive effects of chromium on the catalytic performance are interpreted and discussed.

2. Experimental

2.1. Catalyst preparation

The amorphous Ni–B alloy was prepared by the chemical reduction method, as follows. Seventeen milliliters of aqueous potassium borohydride solution (KBH_4, 2.0 M with 0.10 M of NaOH) was added dropwise into 20.0 ml of nickel chloride aqueous solution ($NiCl_2 \cdot 6H_2O$, 0.42 M) in an ice-water bath. Gentle stirring was maintained throughout the reaction with a magnetic stirrer until no gas was released. The resulting black suspension was centrifuged, and the precipitate was washed thoroughly with oxygen-free distilled water until neutrality and with ethanol for three times to replace water.

The Cr-promoted Ni–B catalysts (denoted as Ni–Cr–B) were prepared in a similar way, except that a certain amount of aqueous potassium chromate solution (K_2CrO_4, 0.48 M) was homogeneously mixed with the $NiCl_2$ solution before the reduction by KBH_4. The amount of chromium in the resulting catalysts can be adjusted by variation of the volume of the chromate solution added.

For comparison, Raney Ni catalyst was prepared by alkali leaching of a commercial Ni–Al alloy (Ni/Al 50/50 w/w) [7]. Since all catalysts can easily be oxidized, care must be taken to avoid their exposure to air. Specifically, Raney Ni with protecting liquid will auto-ignite when directly exposed to air after the liquid is naturally evaporated, and thus is different from Ni–B and Ni–Cr–B catalysts, which ignite only after being dried in vacuo or in inert atmosphere. Generally, the catalysts were kept in ethanol before characterization and activity test.

2.2. Characterization

The bulk compositions of the as-prepared catalysts were determined by inductively coupled plasma-atomic emission spectroscopy (ICP-AES) (Thermo Elemental IRIS Intrepid).

The Brunauer–Emmett–Teller (BET) surface areas were determined by N_2 adsorption at 77 K on a Micromeritics TriStar3000 apparatus with a nitrogen molecule cross section of 0.164 nm^2. Samples with the storage liquid were transferred to the adsorption glass tube and heated at 383 K under ultrahigh pure nitrogen flow for 2.0 h before measurement. Samples were weighed by difference in the adsorption tube on completion of the experiment.

Powder X-ray diffraction (XRD) patterns were acquired on a Bruker AXS D8 Advance X-ray diffractometer with Cu-K_α radiation (40 kV, 40 mA, $\lambda = 0.15418$ nm). Sample with solvent was put in the in situ cell, with argon flow

(99.9995%) purging the sample during the detection to avoid oxidation.

The morphology and particle size were determined by transmission electron microscopy (TEM) (JEOL JEM2011). The amorphous character of the as-prepared Ni–B and Ni–Cr–B catalysts was verified by selected-area electron-diffraction (SAED). Chromium distribution was obtained on an energy-dispersive X-ray emission analyzer (EDX) attached to a scanning electron microscope (SEM) (Philips XL30).

X-ray photoelectron spectroscopy (XPS) (Perkin Elmer PHI5000C) spectra were recorded with the Mg-K_α line as the excitation source ($h\nu = 1253.6$ eV). The sample was pressed into a self-supported disc and mounted on the sample plate. It was degassed in the pretreatment chamber at 383 K for 2 h in vacuo before being transferred into the analyzing chamber, where the background pressure was better than 2×10^{-9} Torr. All of the binding energy (BE) values were obtained after removal of the surface oxides by Ar ion sputtering and referenced to the C 1s peak of contaminant carbon at 284.6 eV with an uncertainty of ±0.2 eV.

H_2 desorption profiles were obtained in the following way. After the samples were treated at 473 K for 2.0 h under argon flow (99.9995%, deoxygenated by an Alltech Oxy-trap filter), they were cooled to room temperature. Deoxygenated H_2 was introduced instead of argon for 1.0 h to ensure the saturation adsorption of hydrogen. The catalyst was then purged with argon to remove gaseous and/or physisorbed hydrogen. The maximum desorption temperature, 873 K, was achieved at a ramping rate of 20 K min^{-1}. The H_2 signal (mass 2) was detected with an on-line mass spectrometer (MS, Stanford SRS 200).

2.3. Activity test and product analysis

An activity test was carried out in a 220-ml stainless steel autoclave with a magnetic stirrer. A mixture of trioctylphosphate and trimethylbenzene (v/v 3/7), the working solution, was used as the solvent, and the concentration of eAQ was 50 g l^{-1}. The reaction conditions were 0.50 g of catalyst, 70 ml of working solution, a H_2 pressure of 0.3 MPa, and a reaction temperature of 323 K. Our preliminary study revealed that the mass transfer limits were readily eliminated at a stirring rate of 1000 rpm.

The reaction process was monitored by sampling of the reaction mixture at intervals, followed by O_2 oxidation. The H_2O_2 produced was extracted from the solution and titrated by $KMnO_4$ in acidic solution. As previously defined [7], the percentage yield X of H_2O_2 is expressed as the ratio of the moles of H_2O_2 to the initial moles of eAQ in the reactor: $X = n^t_{H_2O_2}/n^0_{eAQ} \times 100\%$, which also represents the selectivity to "active quinones." The organic layer left after H_2O_2 extraction was analyzed by high-performance liquid chromatography (HPLC) (Hewlett Packard HP 1100). eAQ and H_4eAQ can be readily quantified by HPLC with an ultraviolet detector and a Zorbax column (ODS 15 cm × 4.6 mm). It is found that under the present reaction conditions only eAQ and H_4eAQ exist, as also confirmed by Finnigan Voyagen GC-MS equipped with an HP-5 capillary column (30 m × 0.25 mm, 0.25 μm).

3. Results and discussion

3.1. Morphological and structural properties of the catalysts

Table 1 lists the compositions and specific surface areas of Raney Ni, Ni–B, and a series of chromium-modified Ni–B samples. According to Table 1, when 1.9 mol% of chromium is incorporated into Ni–B, the B content decreases from 24.4 to 21.3 mol%, and the Ni content increases only slightly as compared with Ni–B. A further increase in the amount of chromium has virtually no effect on the B content, whereas the Ni content decreases proportionally. On the other hand, Table 1 shows that the specific surface area of Ni–B is 32.2 $m^2\,g^{-1}$, about one-third of that of Raney Ni. Incorporation of 1.9 mol% of chromium in Ni–B increases the surface area to 47.9 $m^2\,g^{-1}$. A drastic increment is found for Ni–Cr–B2, which has a surface area fourfold of that of Ni–B. The surface areas of the Ni–Cr–B catalysts then increase moderately when more chromium is incorporated.

Fig. 1 illustrates the typical XRD patterns of Raney Ni, Ni–B, and Ni–Cr–B2 catalysts. For Raney Ni, there are three distinct peaks at Bragg angles of ∼ 44.2°, 51.5°, and 76.1°, corresponding to metallic Ni(111), (200), and (220) planes, respectively [19]. However, for Ni–B and Ni–Cr–B2, there is only one broad peak centered at $2\theta = 45°$, indicating the amorphous structure of the samples [20], which is further evidenced by a diffuse Debye ring rather than distinct dots in their SAED patterns [21].

The morphologies of the amorphous catalysts are observed in Fig. 2 by TEM. From the figure it can be readily concluded that the Ni–B catalyst without chromium exhibits a much larger particle size than does the Ni–Cr–B2 catalyst. As also listed in Table 1, the mean particle size of the Ni–B catalyst is 35 nm, whereas for the Ni–Cr–B1 catalyst, the particle size is 20 nm and then declines to ∼ 7 nm with more chromium incorporated. With the assumption of a spherical shape and nonporous texture of the nanoparticles, a simple

Table 1
Physicochemical properties of the nickel-based catalysts

Catalyst	Composition (atomic ratio)	S_{BET} ($m^2\,g^{-1}$)	d[a] (nm)
Raney Ni	$Ni_{68.0}Al_{32.0}$	98.3	Bulky
Ni–B	$Ni_{75.6}B_{24.4}$	32.2	35
Ni–Cr–B1	$Ni_{76.8}Cr_{1.9}B_{21.3}$	47.9	20
Ni–Cr–B2	$Ni_{75.3}Cr_{3.6}B_{21.1}$	134.7	7
Ni–Cr–B3	$Ni_{70.6}Cr_{8.9}B_{20.5}$	139.0	7
Ni–Cr–B4	$Ni_{64.1}Cr_{14.3}B_{21.6}$	152.5	7

[a] Acquired by TEM.

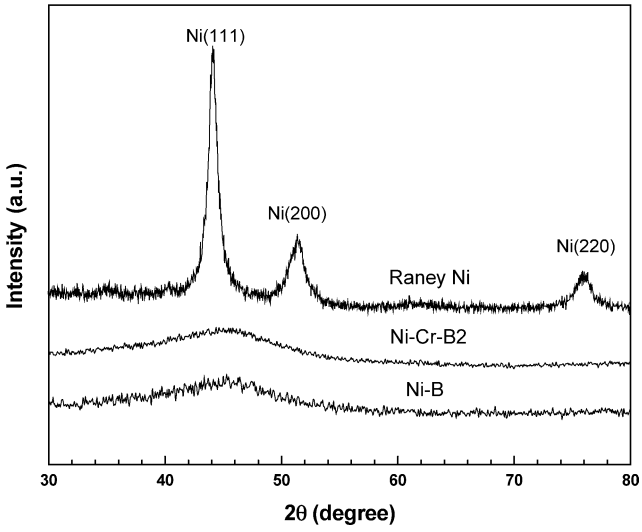

Fig. 1. Powder X-ray diffraction patterns of the Ni–B, Ni–Cr–B2 and Raney Ni catalysts.

calculation reveals that the ratio of the surface areas is the inverse of the ratio of their corresponding particle sizes, which corresponds well with the data listed in Table 1.

EDX experiments were carried out to investigate the distribution of chromium in the Ni–Cr–B catalysts. Boron is not detectable because of the inherent limitation of the technique. A typical result for the Ni–Cr–B2 catalyst is shown in Fig. 3, which demonstrates that the evolution of the concentration of chromium closely follows that of Ni, indicating that chromium is homogeneously dispersed in the catalyst. Moreover, EDX analysis gives a Cr/Ni molar ratio of 0.046 for Ni–Cr–B2 catalyst, which is in good agreement with the chemical analysis result (Table 1).

It is known that because of the high surface energy of the nanosized particles, chemically reduced metal–metalloids, if unsupported or without organic stabilizers, tend to agglomerate with each other to form large particles with diameters of several tens to several hundreds of nanometers [22–26], as in the case shown in Fig. 2a. The addition of chromium seems to be an easy way to reduce the dimension of the Ni–B particles. It should be noted that a smaller particle size does not necessarily mean a reduced thermal stability; however, an additional differential scanning calorimetry (DSC) experiment revealed that the crystallization temperature of Ni–Cr–B2 is 31 K higher than that of Ni–B. Moreover, after the activity test, no increment in the particle size of the Ni–Cr–B catalysts was observed, in compliance with the improved thermal stability of the chromium-promoted nanoparticles.

3.2. *Surface species and electronic properties of the catalysts*

The interaction between Ni and B and the electronic state of chromium are characterized by XPS. From Fig. 4a one can see that almost all of the nickel species in the Ni–B catalyst exist in the elemental state with a Ni $2p_{3/2}$ BE of

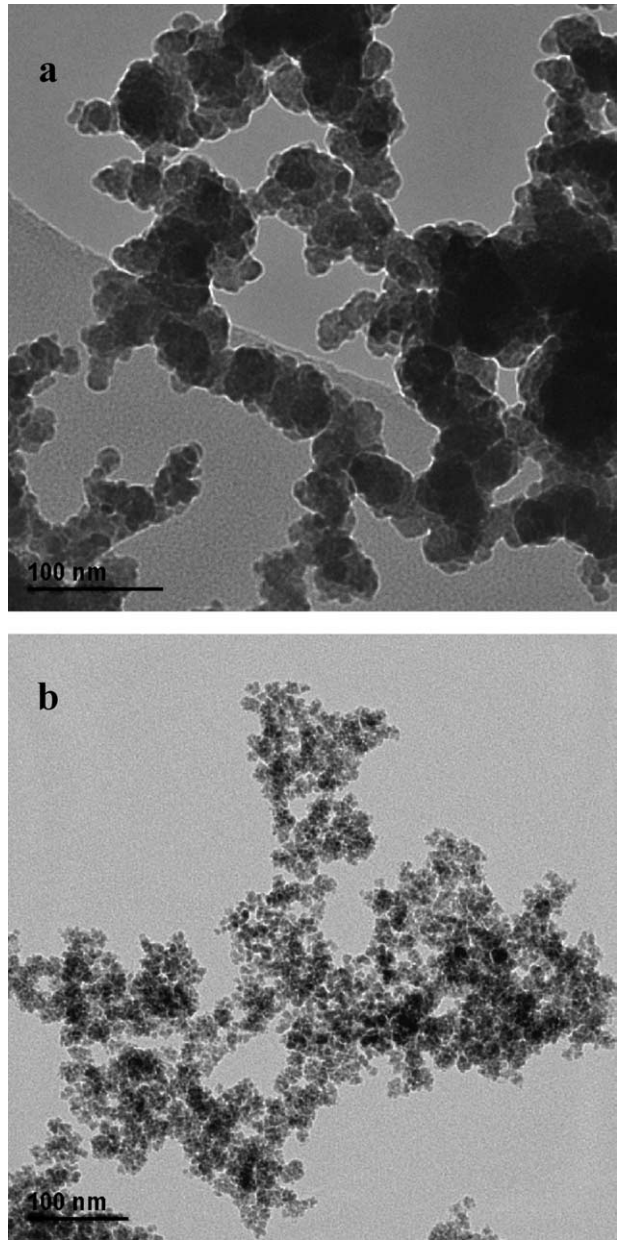

Fig. 2. TEM images of the (a) Ni–B and (b) Ni–Cr–B2 catalysts.

853.0 eV, which is consistent with the $2p_{3/2}$ BE of the reference pure metallic nickel in our experiment, while a small peak at higher BE due to the oxidized nickel species appears and becomes stronger with the increment of chromium content. For both Ni–B and Ni–Cr–B catalysts, the B 1s BE of elemental B is $\sim$ 188.2 eV, about 1.2 eV higher than that of amorphous boron powder [27]. At higher chromium contents, B_2O_3 with B 1s BE of 192.2 eV becomes the dominant B-containing species [27]. On the other hand, the Cr 2p spectrum (Fig. 4b) for Ni–Cr–B catalysts exhibits two peaks at 576.9 and 586.3 eV, ascribable to Cr $2p_{3/2}$ and $2p_{1/2}$ peaks of Cr^{3+} species, respectively [27], showing that Cr^{6+} in K_2CrO_4 can only be reduced to the intermediate valence but not to the elemental state by borohydride.

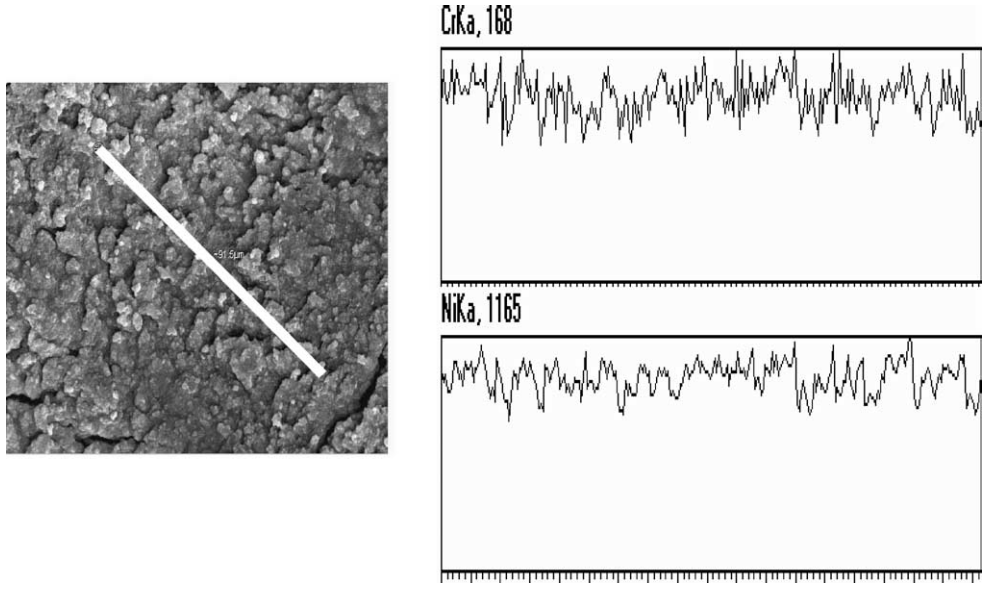

Fig. 3. X-ray line profiles of Ni and Cr in the Ni–Cr–B2 catalyst. The line drawn on the SEM image denotes the range being scanned.

Fig. 4 evidently shows that with the addition of chromium the features of oxidized Ni and B become stronger. A similar phenomenon has been reported by Casagrande et al., who found that for RuCrB catalysts the Ru^0/Ru^{3+} ratio on the catalyst surface decreases as the chromium content increases [28]. For Ni, it is possible that the basic K_2CrO_4 leads to the formation of some nickel hydroxide, which is less reducible than free nickel ions and consequently included in the catalyst. For boron, we assume that K_2CrO_4 alters the acidity of the reduction environment, which may affect the rates of the three independent reactions when borohydride is used as the reducing agent to prepare metal-boron particles: the hydrolysis of borohydride, the reduction of the metal ion, and the reduction of the metalloid, where the first two reactions determine the amount of B_2O_3 in the resulting catalysts [29]. It is also noticed that chromium does not modify the electronic interaction between Ni and B, as their BEs remain unchanged after the addition of chromium.

Based on the above characterizations, we suggest that the Cr^{3+} species, most likely in the form of Cr_2O_3, may locate on the surface of the catalysts, as depicted in Fig. 5. Such surface oxide functions as a partition between Ni–B nanoparticles, which otherwise tend to agglomerate because of their high surface energy, leading to reduced particle size for the chromium-modified Ni–B catalysts. As a result, the thermal stability of the smaller Ni–Cr–B particles remains or is even improved because of the protection of the inert Cr_2O_3 overlayer.

3.3. Catalytic behavior

The relationship between the content of chromium in the amorphous catalysts and the hydrogenation rate (r_{H_2}) of eAQ is illustrated in Fig. 6. r_{H_2} is presented as the hydrogen uptake rate averaged in the first 30 min of the reaction, during which no hydrogenation of the aromatic ring occurs according to the HPLC analysis. The promoting effect of chromium on activity is so drastic that only 1.9 mol% of chromium can double the activity of the Ni–B catalyst. The activity passes the maximum at chromium content of 3.6 mol% and begins to decline slowly at higher contents.

Fig. 7 exhibits the percentage yield of H_2O_2 as a function of time over the Ni–B, Ni–Cr–B2, and Raney Ni catalysts. The evolution of the amount of H_4eAQ during the hydrogenation process is also included. It should be kept in mind that the percentage yield of H_2O_2 virtually denotes the conversion of eAQ to $eAQH_2$ and H_4eAQH_2, whereas H_4eAQ is equal to H_4eAQH_2 in quantity, as illustrated by the reduction-oxidation cycle (Scheme 1). Thus from Fig. 7, the catalytic efficiency of "active quinones" and the selectivity of the catalysts towards the carbonyl group or the aromatic ring can be directly compared.

For Raney Ni Fig. 7a shows that the yield of H_2O_2 reaches its maximum of only 67% at 90 min and drops at prolonged reaction time, implying the formation of the degradation products. H_4eAQ appears as soon as hydrogenation commences, confirming that Raney Ni is not selective in carbonyl group hydrogenation. The decrease in the amount of H_4eAQ at longer reaction time is due to deep hydrogenation of H_4eAQ to H_8eAQH_2, as verified by GC-MS analysis. On the other hand, Fig. 7b shows that over amorphous Ni–B catalyst, the yield of H_2O_2 can be as high as $\sim$ 100% at a reaction time of 180 min. It is worth noting that H_4eAQ does not appear until 60 min and from then on increases very slowly. On amorphous Ni–Cr–B2 catalyst, as depicted in Fig. 7c, the increase in H_2O_2 is much steeper than it is over Ni–B catalyst: only 60 min is needed to achieve 100% yield of H_2O_2. HPLC analysis shows that the amount of eAQ

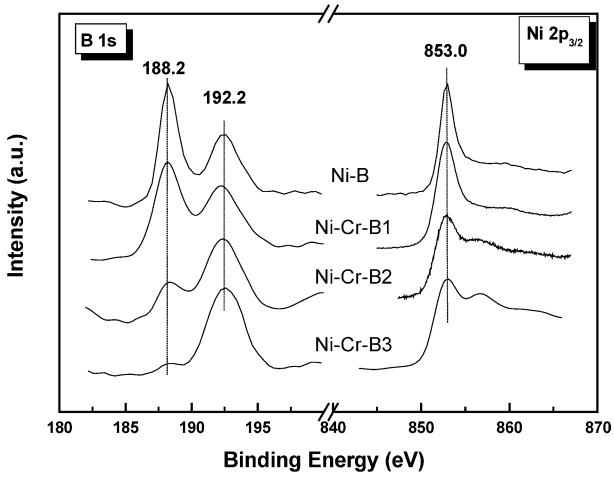

(a)

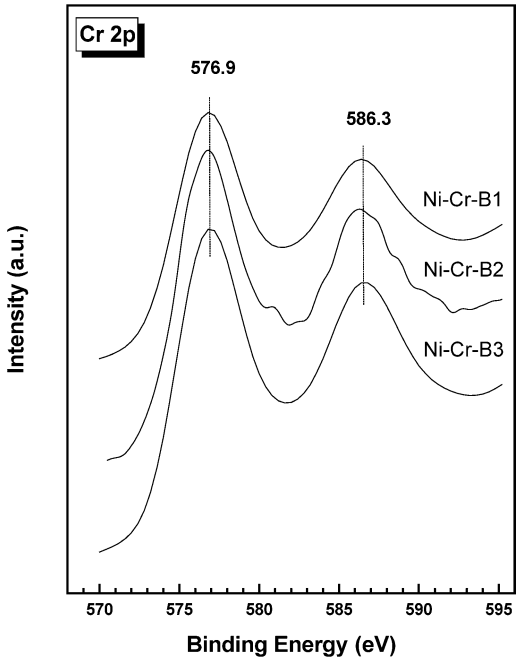

(b)

Fig. 4. The XPS spectra of (a) the B 1s, Ni $2p_{3/2}$ and (b) Cr 2p levels of the Ni–B and Ni–Cr–B catalysts.

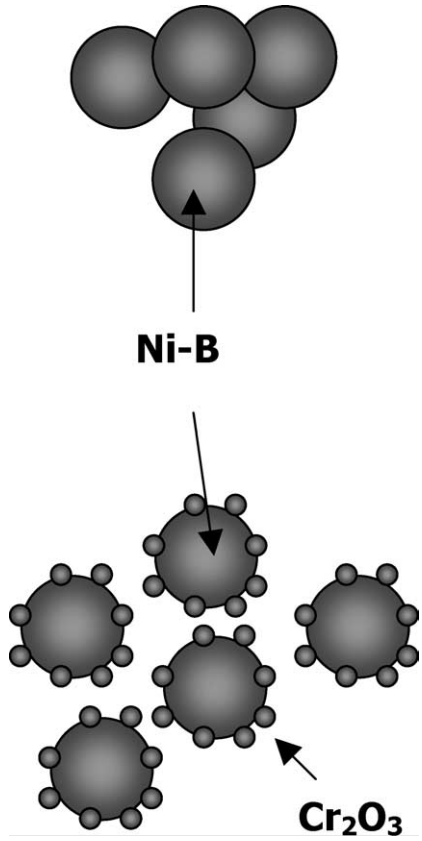

Fig. 5. A model illustrating the modification mechanism of chromium on the Ni–B catalyst.

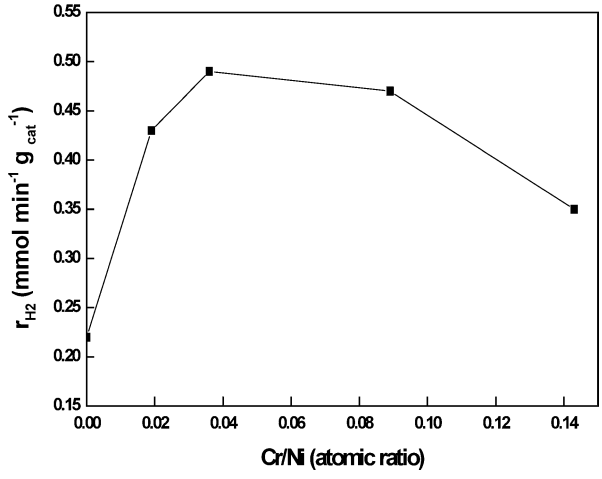

Fig. 6. Influence of the chromium content in the Ni–B and Ni–Cr–B catalysts on the hydrogenation rate r_{H_2} of eAQ averaged in the first 30 min.

remains constant, and no H_4eAQ is detected within the first 60 min. This clearly demonstrates that over Ni–Cr–B2 catalyst hydrogenation of the aromatic ring does not occur if eAQ has not been completely converted to $eAQH_2$. Further reaction leads to the decrement of the amount of eAQ and simultaneously the increment of H_4eAQ. Nevertheless, even after a reaction time of 240 min the amount of eAQ drops by only 10%, whereas the level of products other than "active quinones" is $\sim$ 2%, showing the excellent operability of the as-prepared amorphous Ni–Cr–B2 alloy catalyst.

From Fig. 7 one can readily conclude that amorphous Ni–B and Ni–Cr–B catalysts are less active in aromatic ring hydrogenation than Raney Ni catalyst. The number of H_4eAQ versus time curve can be employed as an indirect measure to compare the selectivities with the carbonyl group over different catalysts. On amorphous catalysts, H_4eAQ forms after a reaction time of $\sim$ 60 min, whereas on Raney Ni catalyst H_4eAQ appears as soon as the reaction begins. On the other hand, although the time for the appearance of H_4eAQ is similar for Ni–B and Ni–Cr–B2 catalysts, the latter is more active and selective in carbonyl group hydrogenation, as we

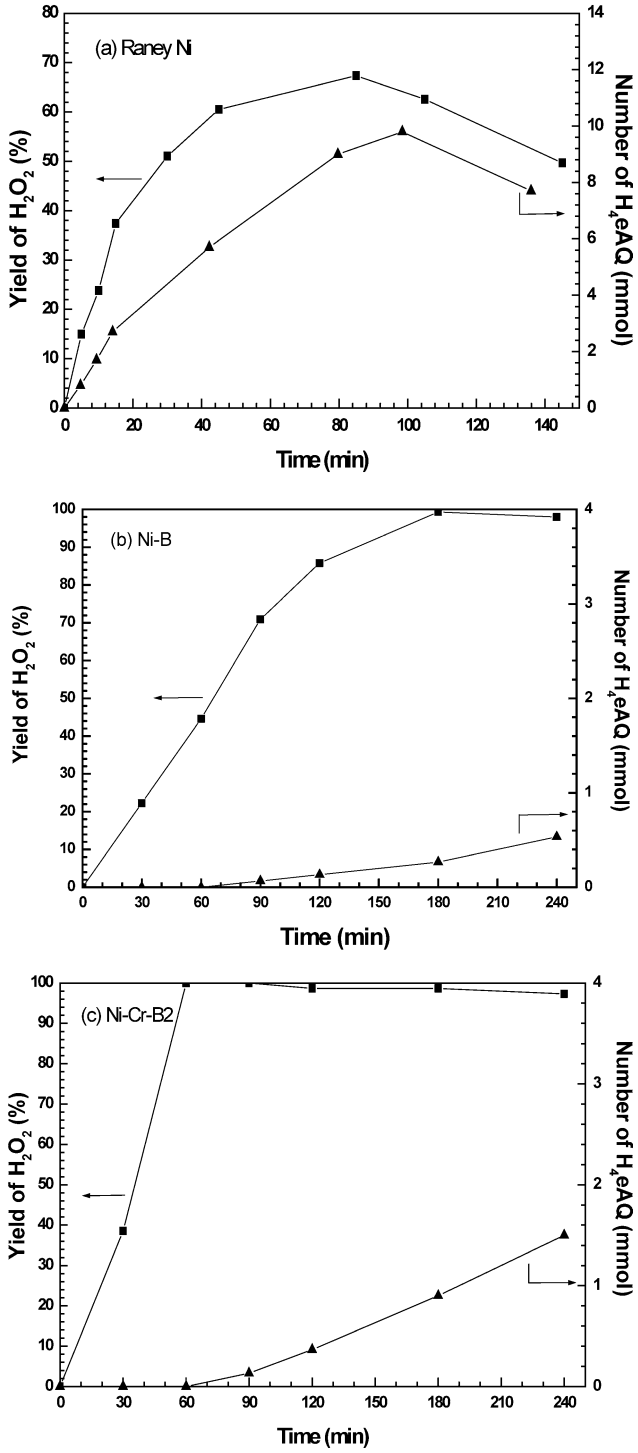

Fig. 7. The percent yield of H_2O_2 and the amount of eAQ and H_4eAQ in the working solution after oxidation as functions of hydrogenation time. (a) Raney Ni, (b) Ni–B and (c) Ni–Cr–B2.

can obtain a 100% yield of H_2O_2 without the formation of H_4eAQ at a reaction time of 60 min.

The inferior selectivity of Raney Ni catalyst in eAQ hydrogenation may be ascribed to the coexistence of weakly bound (at ∼ 450 K) and strongly bound (at ∼ 580 K) hydrogen with comparable populations, as identified by our previous H_2-TPD results [7]. It is acknowledged that a carbonyl group can be hydrogenated by any form of hydrogen, whereas hydrogenation of an aromatic ring demands weakly bound hydrogen [30]. On Ni–B and Ni–Cr–B catalysts the strongly bound hydrogen at ∼ 580 K is dominant, whereas the weakly bound hydrogen at ∼ 450 K is almost indiscernible [18], which is tentatively attributed to the coordinatively unsaturated nature of the amorphous alloys. The difference in hydrogen population is expected to afford superior selectivity in eAQ hydrogenation over amorphous Ni–B and Ni–Cr–B catalysts.

According to the XPS results, the BE of elemental boron positively shifted by 1.2 eV relative to that of pure boron. For metal-rich borides such as NiB, Ni_2B, CoB, Co_2B, and FeB, based on magnetic susceptibility, ^{59}Co NMR, and high-resolution Bremsstrahlung isochromat measurements, it is suggested that B donates electron to metal [31]. The BE shift of B in our case can be interpreted in a similar manner. We did not observe the BE shift of nickel alloying with boron, as a rough calculation indicates that Ni $2p_{3/2}$ BE shifts negatively only by ∼ 0.07 eV in Ni–B and Ni–Cr–B alloys [32], far below the experimental error of ±0.2 eV. Thus B in Ni–B and Ni–Cr–B catalysts may act as an electron-donating ligand to Ni and consequently decrease the binding strength between the aromatic ring and Ni due to enhanced electronic repulsive interaction [33], leading to a decrease in the hydrogenation of the aromatic ring. Moreover, the electron donation of B to Ni strengthens the adsorption of the carbonyl by increasing the back-donation into π^*_{CO}. The double roles of B result in an increased selectivity to the hydrogenation of the carbonyl group in eAQ.

According to BET and TEM, the better activity of the Ni–Cr–B catalysts than that of the unmodified Ni–B catalyst is ascribed to the reduced particle size by the incorporation of chromium oxide, exposing more active sites for eAQ hydrogenation. But XPS reveals that excessive chromium oxide reduces the amount of surface elemental Ni and B and may block the active sites; thus an optimal concentration of the chromium additive exists, as confirmed by Fig. 6. On the other hand, in the case of catalytic hydrogenation, it is generally assumed that the reactive bond is the one involved in chemisorption on the surface [17,34]. By a systematic theoretical calculation, Delbecq and Sautet suggested that the main attractive effect in the adsorption of aldehyde on surfaces is the back-donation from the metal orbitals into π^*_{CO}. When this orbital is shifted down, the interaction is better and the adsorption is stronger. And they pointed out that the shift can be achieved by complexation of the carbonyl group with Lewis acids [33]. Following their idea, we propose that the surface chromium oxide in the Ni–Cr–B catalysts can act as a Lewis acid site and improve the adsorption and the reactivity of the carbonyl groups relative to the aromatic ring, which well explains the exclusive selectivity in the hydrogenation of the carbonyl groups in eAQ over the Ni–Cr–B2 catalyst as compared with that of the unmodified Ni–B catalyst.

4. Conclusion

Amorphous Ni–B and Ni–Cr–B catalysts are superior to Raney Ni in selective hydrogenation of eAQ to $eAQH_2$ for H_2O_2 production, which can be accounted for by the dominant population of the strongly bound hydrogen and the unique electronic structure of the amorphous metal boride catalysts. The electron donation of B to Ni not only decreases the adsorption of the aromatic ring, but also strengthens the adsorption of the C=O group by increasing the backdonation into π^*_{CO}, thus resulting in increased selectivity to carbonyl hydrogenation. The effects of chromium on the catalytic performance of the amorphous Ni–B catalyst are twofold. One is that the chromium oxide promotes the catalytic activity by retarding the agglomeration of the nanoparticles and consequently increasing the active surface area for hydrogenation. The other is that it functions as a Lewis acid, which directs the adsorption of eAQ in the carbonyl group-bonded configuration on the catalyst, thus thoroughly suppressing the hydrogenation of the aromatic ring.

Acknowledgments

This work is supported by the State Key Basic Research Development Program (G2000048009), the NSF of China (20203004), and the Shanghai Science and Technology Committee (03QB14004).

References

[1] C.S. Cronan, Chem. Eng. 66 (1959) 118.
[2] T. Ulmann (Ed.), Encyclopedia of Industrial Chemistry, vol. A3, VCH, Weinheim, 1989, p. 443.
[3] J.I. Kroschwitz, M. Howe-Grant (Eds.), Kirk–Othmer Encyclopedia of Chemical Technology, vol. 13, fourth ed., Wiley, New York, 1995, p. 961.
[4] A. Drelinkiewicz, M. Hasik, M. Kloc, Catal. Lett. 64 (2000) 41.
[5] A. Drelinkiewicz, J. Mol. Catal. 101 (1995) 61.
[6] E. Santacesaria, M. Di Serio, R. Velotti, U. Leone, J. Mol. Catal. 94 (1994) 37.
[7] B. Liu, M.H. Qiao, J.F. Deng, K.N. Fan, X.X. Zhang, B.N. Zong, J. Catal. 204 (2001) 512.
[8] G. Kisfaludi, K. Lazar, Z. Schay, L. Guczi, Cs. Fetzer, G. Konczos, A. Lovas, Appl. Surf. Sci. 24 (1985) 225.
[9] M. Peuckert, A. Baiker, J. Chem. Soc., Faraday Trans. 1 81 (1985) 2797.
[10] H. Yamashita, M. Yoshikawa, T. Funabiki, S. Yoshida, J. Chem. Soc., Faraday Trans. 1 82 (1986) 1771.
[11] H.X. Li, W.J. Wang, H. Li, J.F. Deng, J. Catal. 194 (2000) 211.
[12] J.F. Deng, Curr. Top. Catal. 2 (1999) 1.
[13] P. Gallezot, P.J. Cerino, B. Blanc, G. Flèche, P. Fuertes, J. Catal. 146 (1994) 93.
[14] J. Masson, P. Cividino, J. Court, Appl. Catal. A 161 (1997) 191.
[15] H. Li, H.X. Li, J.F. Deng, Catal. Today 74 (2002) 53.
[16] Y.Z. Chen, S.W. Wei, Appl. Catal. 99 (1993) 85.
[17] V. Ponec, Appl. Catal. A 149 (1997) 27.
[18] B. Liu, M.H. Qiao, J.Q. Wang, K.N. Fan, Chem. Commun. (2002) 1236.
[19] S.D. Robertson, J. Freel, R.B. Anderson, J. Catal. 24 (1972) 130.
[20] J. Wonterghem, S. Mørup, S.W. Charles, S. Wells, Nature 322 (1986) 622.
[21] T. Osaka, K. Arai, N. Masubuchi, Y. Yamazaki, T. Namikawa, Jpn. J. Appl. Phys. 28 (1989) 866.
[22] J. Jiang, I. Dézsi, U. Gonser, J. Weissmüller, J. Non-Cryst. Solids 116 (1990) 247.
[23] Z. Hu, Y.F. Hsia, J.G. Zheng, J.Y. Shen, Q.J. Yan, L.M. Dai, J. Appl. Phys. 70 (1991) 436.
[24] S. Mørup, S.A. Sethi, S. Linderoth, C. Benderkoch, M.D. Bentzon, J. Mater. Sci. 27 (1992) 3010.
[25] S.P. Lee, Y.W. Chen, Ind. Eng. Chem. Res. 40 (2001) 1495.
[26] P. Fulmer, M.M. Raja, A. Manthiram, Chem. Mater. 13 (2001) 2160.
[27] Handbook of X-ray Photoelectron Spectroscopy, Perkin Elmer Corporation, 1992.
[28] M. Casagrande, L. Storaro, A. Talon, M. Lenarda, R. Frattini, E. Rodríguez-Castellón, P. Maireles-Torres, J. Mol. Catal. A 188 (2002) 133.
[29] Y. Chen, Catal. Today 44 (1998) 3.
[30] S.D. Mikhailenko, A.B. Fasman, N.A. Maksinova, E.V. Leongard, Appl. Catal. 12 (1984) 141.
[31] Y. Okamoto, Y. Nitta, T. Imanaka, S. Teranishi, J. Chem. Soc., Faraday Trans. 1 15 (1979) 2027.
[32] J. Li, M.H. Qiao, J.F. Deng, J. Mol. Catal. A 169 (2001) 295.
[33] F. Delbecq, P. Sautet, J. Catal. 152 (1995) 217.
[34] T.B.L.W. Marinelli, S. Nabuurs, V. Ponec, J. Catal. 151 (1995) 431.